

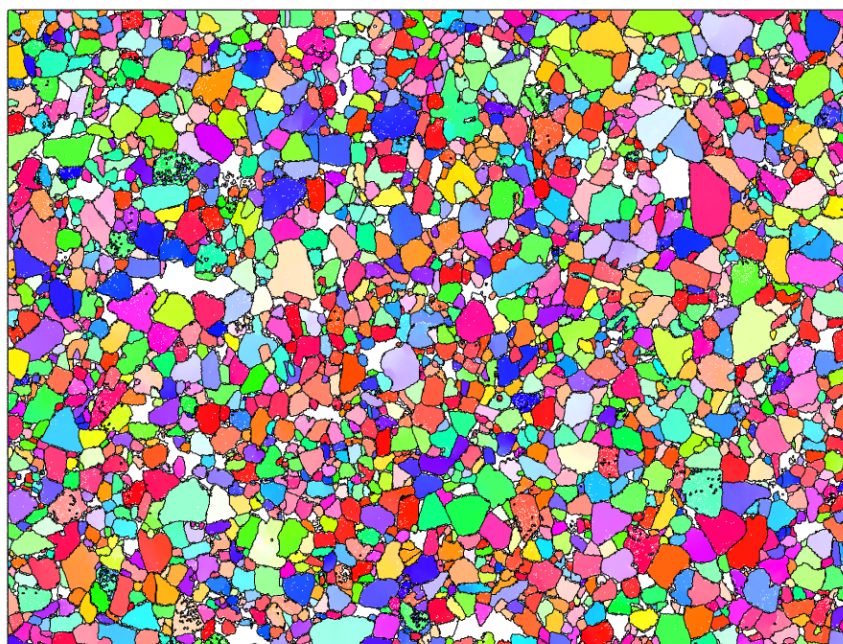


Department of Materials Science and Engineering, KTH Royal Institute of Technology  
MH101X VT25 Examensarbete inom material- och processdesign grundnivå 15 hp

# Mechanical properties of cemented carbides with an alternative binder

The effects of varying initial WC powder particle sizes

Axel Magnusson, Rose Cuvillon, Simon Bonn



TRITA - ITM-EX 2025:284  
Stockholm, Sweden 025

[www.kth.se](http://www.kth.se)

# Abstract

Most modern cemented carbides use cobalt binders, but recent research has attempted to partially or totally replace cobalt in the binder due to its carcinogenicity and negative impact on the climate. This thesis examines the mechanical properties of a tungsten-based cemented carbide with an alternative iron-nickel-cobalt binder. The investigations are carried out on 4 samples, provided by Sandvik Mining & Rock Solutions, with varying initial tungsten carbide particle sizes. The hardness of the samples was measured using the Vickers hardness tests, and the microstructure was examined with Light Optical Microscopy (LOM) and Electron Backscatter Diffraction (EBSD). These experimental measurements resulted in hardness values, average grain size values, and qualitative toughness values using the crack lengths from the Vickers hardness test. The results confirmed previous studies showing that hardness is proportionally linked to the amount of iron in the binder, and inversely proportional to the average grain size and the toughness of the cemented carbide. Furthermore, it showed that iron-nickel-cobalt binders promote a more complex phase composition, with smaller grains and the possibility of Transformation Induced Plasticity (TRIP) effects for improved toughness. These findings support the viability of iron-nickel-cobalt binders as a sustainable alternative to traditional cobalt binders, offering promising mechanical properties for demanding applications such as rock drilling.

# Sammanfattning

De flesta moderna hårdmetaller använder koboltbindefas, men nyare forskning har försökt att helt eller delvis ersätta kobolt i bindemedlet på grund av dess karcinogenicitet och negativa klimatpåverkan. Denna avhandling undersöker de mekaniska egenskaperna hos volframbaserad hårdmetall med ett alternativt järn-nickel-kobolt-bindemedel. Undersökningarna har genomförts på 4 prover, tillhandahållna av Sandvik Mining & Rock Solutions, med samma sammansättning men varierande initial partikelstorlek på volframkarbiden. I genomförandet utfärdades Vickers hårdhetstest samt mikroskopianalyser med ljusoptisk mikroskopi (LOM) och bakåtspridd elektronndiffraktion (EBSD) på tvärsnittet av proverna. Resultaten från experimenten gav värden för hårdhet, kornstorlek och brottseghet baserat på spricklängder från intrycken av hårdhetstesterna. Dessa resultat bekräftar tidigare studier som visar att hårdheten är proportionell mot mängden järn i bindemedlet samt omvänt proportionell mot kornstorlek och brottseghet. Vidare visade det sig att järn-nickel-kobolt främjar en mer komplex fassammansättning, med mindre korn och möjligheten till Transformation Induced Plasticity (TRIP)-effekter för förbättrad brottseghet. Resultaten stödjer användbarheten av järn-nickel-kobolt som ett mer hållbart alternativ till kobolt, med lovande mekaniska egenskaper för krävande applikationer såsom bergborrning.

# Table of contents

<b>1 Introduction</b>	<b>1</b>
<b>2 Literature study</b>	<b>2</b>
2.1 Microstructure of cemented carbides	2
Traditional WC-Co cemented carbides	2
Alternative Fe-Ni-Co binders	2
2.1.1 WC powder particle size	3
2.1.2 Contiguity	3
2.1.3 Tungsten carbide grain growth	3
2.1.5 Undesirable carbon phases	4
Carbon window	4
Eta-phase	4
Graphite phase	5
2.2 Manufacturing cemented carbides	5
2.2.1 Milling	5
2.2.2 Pressing	5
2.2.3 Sintering	5
2.3 Mechanical properties of cemented carbides	6
2.3.1 Hardness	6
2.3.2 Fracture toughness	6
2.3.3 Hardness-toughness dichotomy	7
<b>3 Experimental</b>	<b>9</b>
3.1 Sample production and preparation	9
3.2 Vickers hardness test	9
3.3 Fracture toughness	10
3.4 Light optical microscopy	10
3.5 Scanning electron microscopy	10
3.5.1 Broad Ion Beam	10
3.5.2 Electron backscatter diffraction	11
3.5.3 Post-processing EBSD data	11
<b>4 Results</b>	<b>12</b>
4.1 Phase diagram	12
4.2 Hardness	13
4.3 Fracture toughness	13
4.4 Grain size	14
<b>5 Discussion</b>	<b>18</b>
5.1 Obtained results	18
5.2 Discussion on hardness results	18
5.3 Discussion of crack length and fracture toughness	21
5.4 Sources of errors	23
5.5 Social and ethical aspects	23
<b>6 Conclusions</b>	<b>24</b>
<b>7 Future work</b>	<b>25</b>
<b>8 Acknowledgment</b>	<b>26</b>
<b>9 References</b>	<b>27</b>
<b>Appendix</b>	<b>30</b>

# 1 Introduction

Cemented carbides are a class of cemented cermet materials composed of ceramic particles surrounded by a sintered metal matrix. The most common ceramics in cemented carbides are tungsten carbide (WC), titanium carbide (TiC), and silicon carbide (SiC), where this thesis report will focus on tungsten carbide grades. The metal matrix, commonly known as the metallic binder phase, traditionally consists of cobalt (Co). Cemented carbides are widely used in the mining industry for rock drilling and grinding applications, thanks to their outstanding combination of hardness and toughness. Cemented carbide drill bit buttons are manufactured through powder metallurgy, where WC and Co raw materials are mixed in a tumbler mill to form a homogeneous powder. The powder is pressed into the desired drill bit shape and sintered to form a dense and hard cemented carbide. Sintering is a heat treatment and densification process that melts the metallic binder around the tungsten carbide grains. Various microstructures with distinct mechanical properties can be achieved by adjusting the composition and particle size of the ingoing raw material.

In recent times, there has been a shift toward creating cemented carbides with alternative metallic binder phases to decrease the dependency on cobalt. Cobalt mining is highly controversial both environmentally and ethically, albeit necessary for producing EV batteries, consumer electronics, and the aviation industry. The demand for cobalt will increase drastically to reach the goal of net-zero carbon emissions by 2050. [1] Therefore, alternative metals must be used to the greatest extent possible so that cobalt consumption can be reduced and limited to applications where it is irreplaceable.

Sandvik Mining & Rock Solutions has prepared 4 cemented carbide samples with a new alternative metallic binder, a Fe-Ni-Co alloy with 50 wt% Fe, 25 wt% Ni, and 25 wt% Co. This thesis aims to evaluate the mechanical properties of cemented carbides with the alternative metallic binder alloy, and how different ingoing tungsten carbide raw material particle sizes affect the final properties of the cemented carbide. The alternative cemented carbide samples have been prepared using the same manufacturing conditions as Sandvik's traditional cemented carbide with a pure cobalt binder. The ingoing raw material plays a crucial role in the final microstructure of the cemented carbide. By analyzing the microstructures of the four cemented carbide samples, valuable insights can be gained regarding the influence of tungsten carbide particle size on the material's mechanical properties. A detailed microstructural evaluation and mechanical testing can provide a deeper understanding of the relationship between composition, processing parameters, and final material performance.

This knowledge is essential for optimizing the design and manufacturing of future cemented carbides and developing materials with enhanced mechanical properties for improved performance in rock drilling applications. Furthermore, the findings from this study can contribute to the broader research on alternative metallic binders, supporting the transition towards more sustainable and efficient solutions in the cemented carbide industry.

## 2 Literature study

### 2.1 Microstructure of cemented carbides

#### *Traditional WC-Co cemented carbides*

The primary phase in cemented carbides is tungsten carbide (WC), which provides the exceptional hardness and wear resistance characteristic of these materials. WC has a simple hexagonal (SH) crystal structure and has a very narrow range of homogeneity around its stoichiometric composition (approximately 6.13 wt% C) [2]. The secondary phase is the metallic cobalt (Co) binder, which cements the WC grains together. The binder content can range from 3-30 wt%, although most cemented carbide grades contain 6-20 wt% binder. The Co binder phase provides ductility and toughness to the material and facilitates sintering thanks to its excellent wettability with WC. The Co binder crystal structure is influenced by dissolved tungsten and carbon, and the cooling rate after sintering. Pure cobalt normally transforms from a high-temperature face-centered cubic (FCC) structure to a low-temperature hexagonal close-packed (HCP) below 427°C, but the dissolution of W and C into the Co binder during sintering increases the stacking fault energy and stabilizes the FCC phase, allowing it to remain at room temperature. This retained FCC phase results in improved toughness and transverse rupture strength [3]. Manipulating the W and C solubility, and thereby the FCC/HCP phase balance, through rapid cooling to retain the supersaturated FCC-Co provides a method to improve the mechanical properties of the cemented carbide. The WC grains in well-sintered WC-Co cemented carbides have a distinct morphology: A truncated trigonal prism shape with flat crystallographic facets [2].

A cemented carbide piece for rock drilling applications may show a gradient between different microstructural zones. The surface zone has a higher fraction of WC and reduced binder content to increase the hardness, while the intermediate region has higher binder content to increase the toughness. In the bulk region, there are WC and average binder content with precipitation of  $\eta$ -phase. This binder gradient generates a compressive stress that prevents crack propagation. [2]

#### *Alternative Fe-Ni-Co binders*

Substituting conventional Co binder with alloy-based binder of Fe, Ni, and Co results in notable differences in the microstructure and can offer both benefits and new complexities.

The most notable difference is in the binder phase. Unlike the stable FCC structure of the Co binder, the Fe-Ni-Co binder has a structure that is highly sensitive to its composition, and particularly the Fe/Ni ratio. The binder phase tends to transition from FCC  $\gamma$ -(Fe,Ni) to body-centered cubic (BCC)  $\alpha$ -(Fe,Ni) with increasing Fe content relative to Ni (and a constant Co content) [4]. Depending on the composition and heat treatment, the binder can exist as a single phase (FCC or BCC), a mixture of the two, or undergo a martensitic transformation (FCC  $\rightarrow$  BCC or FCC  $\rightarrow$  BCT) when cooled or subjected to mechanical stress. This potential martensitic transformation can induce a transformation toughening effect, enhancing the fracture toughness. [5]

Fe-Ni-Co-based binders, like Co binders, have good wettability with WC. This promotes densification during the liquid phase sintering process and allows for the production of close to fully dense materials. The specific composition of the alternative Fe-Ni-Co binder influences the morphology and

distribution of the WC grains in the microstructure. It is suggested that increasing Fe content relative to Ni tends to promote the formation of finer and more rounded WC grains with a more uniform distribution within the matrix [4]. Iron seems to have an inhibitory effect on WC grain growth during sintering, which could help achieve a finer microstructure than what is possible with WC-Co binders with the same sintering conditions. Nickel, on the other hand, might favor the development of more angular, prismatic WC grains similar to those of WC-Co [5], [4].

### 2.1.1 WC powder particle size

There is a strong correlation between the average particle size of the WC powder and the grain size of the WC phase. Finer initial powders (nano <0,2 µm, up to fine <1,3 µm) generally result in a finer-grained microstructure, while coarser starting powders (medium >1,3 µm to extra coarse >6,0 µm) lead to a coarser microstructure [6] [7].

The average WC grain size impacts the binder mean free path (MFP), essentially the thickness of the binder phase. Finer WC grains result in a shorter average distance between the grains in the binder phase and thereby a lower MFP, while coarser grains lead to longer distances between grains and a higher MFP [7].

During a cutting test, fine particle powder has the lowest cutting-edge wear rate and mass loss, due to a better volume repartition of the grains. The finer the WC particles are, the harder and more wear-resistant the cemented carbide is. [8]

### 2.1.2 Contiguity

Contiguity is an important microstructural parameter in cemented carbides. It quantifies the extent of direct tungsten carbide to tungsten carbide (WC/WC) grain contact. It leads to the formation of a continuous, three-dimensional network of WC grains, often described as the “WC skeleton” [9].

The degree of contiguity, and thus the development of the WC skeleton, is primarily governed by the volume fraction of the binder phase. There is a strong inverse linear correlation between these two parameters. A higher binder phase volume fraction naturally leads to a larger separation between WC grains, which reduces the opportunities for direct WC/WC grain contacts, resulting in lower contiguity [10].

Conversely, reducing the binder content promotes more frequent contact between the WC grains, which increases the contiguity. While contiguity focuses on the WC grain network, the characteristics of the binder phase distribution are also important. The binder mean free path (MFP) is a related parameter used to describe the average distance across the binder phase separating adjacent WC grains. It provides a measure of the average thickness or spacing of the binder network between the carbide grains. Interestingly, while the amount of binder plays a crucial role in determining the contiguity, it has been shown that the average size of the WC grains does not have a significant influence on the overall WC contiguity [11].

### 2.1.3 Tungsten carbide grain growth

The WC grain growth is predominantly driven by Oswald ripening during liquid phase sintering. Smaller, higher energy WC particles dissolve into the liquid binder, and subsequently diffuse and reprecipitate onto larger, lower energy grains [2]. Finer initial WC powder particles have a higher total

surface area and surface energy, which increases the driving force for sintering and grain growth. As a consequence, systems with finer starting powders have a higher sintering activity, meaning densification and grain growth tend to start at lower temperatures than systems with coarser powders. This makes fine-grained systems more susceptible to abnormal grain growth, where a few grains grow disproportionately large [7]. To counteract this excessive coarsening when using ultra-fine powders, grain growth inhibitors (GGIs) can be utilized. They work by various mechanisms, such as altering WC/binder interfacial energy, segregating to the interfaces, physically hindering boundary migration, or modifying diffusion pathways in the binder. As mentioned earlier, Fe-rich binders can provide grain growth inhibition and result in finer grain sizes. [4] [6].

The Lifshitz–Slyozov–Wagner (LSW) theory explains grain growth with two main processes, diffusion control and interface reaction control. The driving force for grain growth is lower in systems with spherical grains, which results in normal grain growth (NGG). However, since WC grains have a prismatic shape, they have more ordered, singular interfaces, and atom attachment on these singular interfaces requires a significantly higher driving force. This leads to the necessity of additional mechanisms, such as the formation of 2-D nuclei or surface defects, to facilitate growth. Only the grains with a sufficient driving force can overcome this barrier when the driving force for grain growth exceeds a critical threshold. As a result, a few grains grow significantly larger while the rest show little to no growth, which leads to abnormal grain growth (AGG) [12]

### 2.1.5 Undesirable carbon phases

#### *Carbon window*

Carbon content in cemented carbides is crucial for determining the phase equilibrium and microstructure. The optimal "carbon window" is defined by the WC-Co phase equilibrium, where the carbon-to-tungsten ratio at a given temperature and cobalt content determines which phases are present. The two-phase system of WC and Co is maintained in a narrow window, and small deviations in carbon content can drastically change the properties of the cemented carbide. Excess carbon leads to the crystallization of graphite, which creates a three-phase equilibrium of WC- $\beta$ -graphite in the solid regions of the phase diagram, where  $\beta$  is the binder phase. or WC–liquid–graphite above the liquidus line. Carbon deficiency results in the formation of eta-phase ( $\eta$ -phase) in the form of two different carbides,  $M_6C$  or  $M_{12}C$  [2].

The amount of carbon in the cemented carbide can be referred to as the carbon balance of the alloy (equal to 0 in stoichiometric conditions). That balance can be influenced by the initial carbon content; the oxygen content, because oxygen reacts with carbon during sintering, reducing the amount of carbon; and the debinding process during sintering, which can reduce the carbon content.

The solubility of tungsten in liquid cobalt decreases with increasing carbon activity. More tungsten dissolves in the binder when the carbon content is low. The exact carbon content required also depends on the overall alloy composition and binder type. The inclusion of Fe in the binder narrows the carbon window, which makes manufacturing more sensitive, while Ni behaves more similarly to Co, and conversely, widens the carbon window. [13]

#### *Eta-phase*

The  $\eta$ -phase is a brittle and undesirable carbon-deficient form of tungsten carbide, which decreases the toughness of the cemented carbide. It is a ternary carbide that contains W, Co, and C and forms

during sintering when the carbon activity is too low and the cemented carbide decarburizes.  $\eta$ -phase has the structures  $M_6C$  and  $M_{12}C$  (where  $M = W$  and binder metal) that both crystallize under a cubic structure. It precipitates under a dendritic structure, which is problematic for mechanical properties. The amount of  $\eta$ -phase in the alloy depends on the carbon deficiency and the cooling rate, where  $M_6C$  is more likely to appear than  $M_{12}C$  with a faster cooling rate:

- Extremely minor carbon deficiency:  $\eta$ -phase can completely disappear during the cooling.
- Minor carbon deficiency:  $\eta$ -phase nucleates upon cooling, creating large brittle areas. Theoretically, the  $\eta$ -phase can decompose, but it is a slow process, and it may remain in the microstructure, so that carbon content tends to be avoided.
- High carbon deficiency:  $\eta$ -phase is already present at the sintering temperature, it remains in the structure after cooling, in the form of finely dispersed particles. The higher the deficiency, the bigger the particle size and the volume fraction. [2]

### *Graphite phase*

Contrary to the  $\eta$ -phase, graphite can form in cemented carbides with a high carbon activity as graphite flakes or inclusions. Like the  $\eta$ -phase, it is undesirable in cemented carbides as it degrades the mechanical properties [2].

## 2.2 Manufacturing cemented carbides

### 2.2.1 Milling

Milling is the first step in the manufacturing process of cemented carbides, where the ingoing raw material is mixed with a milling liquid and a grinding and binding aid. The purpose of the milling process is to obtain a homogeneous powder mixture with a desired particle size. The milling liquid is generally an alcohol that protects the powder from oxidation. Since the powder particles have an order of magnitude of 1  $\mu\text{m}$  or smaller, the particles can spontaneously form an agglomerate. A controlled agglomeration can be initiated to avoid this, which creates spherical granules with an order of magnitude of ca 100  $\mu\text{m}$  that are easier to control [14]. Another method is ball milling, which works by placing grinding balls in the mill along with the raw material. Under high rotational speed, the balls crush the material until it forms a homogeneous powder. Different powder particle diameters can be necessary depending on the application of the cemented carbide. To do so, one can vary the parameters, like the size of the milling balls, the rotation speed, the balls-to-powder ratio in the cylinder, the medium of milling, and the milling time.

[15]

### 2.2.2 Pressing

The milled powder of WC and binder is placed in a mould, a cap closes the mould and applies strong pressure to the powder so that it agglomerates and forms a green body in the desired shape of the final cemented carbide drill bit. The green body is highly porous but solid enough to be handled.

### 2.2.3 Sintering

The sintering process is a heat treatment and densification process that removes all the porosity in the green body through different diffusion processes. A reduction in surface energy is the driving force for the reaction. Cemented carbide powder is put in the sintering furnace under the shape it was pressed,

it doesn't need to be placed in a mould to keep its form, as the essence of sintering is to form a single solid mass with high pressure and temperature without reaching the liquidation point.

During sintering, the microstructure and the mechanical properties can be adjusted by the conditions such as temperature, pressure, contaminants in the atmosphere, heating/cooling rates, and the duration of sintering. For cemented carbides, sintering happens in four main steps. First, there is shrinkage due to degassing of the polymer binder. Then, the solid state sintering happens, and the binder phase wets the WC grains. Porosity decreases and densification increases. The dissolved material in the binder reprecipitates the grains that didn't dissolve. In the third step, liquid phase sintering happens as the melting point of the binder phase is reached, and grains are dissolved in the binder to saturation. The larger grains grow at the expense of the smaller ones, which are dissolved. Only the binder melts, as the WC remains solid and retains the green body shape. During the fourth step, the phase solidifies due to cooling. On leaving the furnace, the cemented carbide ends have greatly shrunken, up to a reduction of more than 50% of the initial volume.

## 2.3 Mechanical properties of cemented carbides

### 2.3.1 Hardness

Hardness is a measure of a material's resistance to plastic deformation. It can be measured with numerous methods, with the Vickers method being the most common for cemented carbides. The Vickers hardness test works by indenting the surface of a material with a pyramid-shaped diamond indenter at a constant angle. This simplifies the calculations and minimizes hardness variations when different loads are applied. The hardness value is a ratio of the applied force (kgf) and the indentation surface area ( $\text{mm}^2$ ), and is written as 1000HV20, where 1000 is the Vickers hardness ( $\text{kgf}/\text{mm}^2$ ) and 20 is the applied force. High hardness is essential for rock drilling applications as it resists the abrasive action of rock particles, minimizes wear, and maintains the tool's geometry.

Cemented carbides generally have a Vickers hardness value between 700 and 2200 HV30. This wide range depends on several factors, like binder to carbide ratio, binder composition, and grain size. Increased binder content generally decreases hardness due to the reduced volume fraction of the hard WC [16]. Fe-Ni-Co binders can achieve similar, and in some cases, exceeding hardness levels compared to traditional WC-Co grades with similar WC content and grain size. This can be attributed to factors like the inherent hardness of the Fe-Ni-Co binder phase due to its FCC/BCC/martensite structure, or finer WC grain size due to the growth inhibition of Fe. On the contrary, some alternative binders can decrease the hardness due to a larger binder mean free path or lower inherent hardness compared to Co. Decreasing the average WC grain size leads to a significant increase in hardness [2]. This can be described by the Hall-Petch relationship, where hardness is inversely proportional to the square root of the grain size or binder mean free path. [17]

### 2.3.2 Fracture toughness

Fracture toughness is the resistance of a material to the propagation of cracks under a stress. The plane strain fracture toughness,  $K_{IC}$ , is the critical factor for conditions where brittle fractures are a concern. The ductile binder phase significantly improves the fracture toughness compared to the brittle ceramic phase. Typical  $K_{IC}$  values for WC-Co cemented carbides range between 7-25 MPa/m<sup>1/2</sup> [15]. It varies greatly depending on the microstructure of the cemented carbide, particularly the WC grain size and

binder content. Increased fracture toughness often comes at the expense of hardness. Fracture toughness increases, and hardness decreases with increasing WC grain size and binder content. [18]

Fracture toughness can be enhanced through different mechanisms, with the two most significant being crack deflection and ductile ligament bridging. Crack deflection is where the crack front is forced to deviate from its planar path when it meets an obstacle in the microstructure. In cemented carbides, the obstacle is the hard WC grains. When the crack meets a large WC grain, it is energetically favorable for the crack to deflect and propagate around the grain through the softer binder phase, rather than cleaving directly through the WC grain. [19] Since the crack has to travel a longer distance, it requires a higher energy input, thereby increasing the material's fracture toughness. Larger grains present higher barriers for planar crack propagation, and therefore, larger grains increase the fracture toughness [20].

Ductile ligament bridging is a mechanism where the ductile binder phase does not fracture immediately with the crack front. Instead, it stretches across the crack faces behind the crack tip, forming ligaments that exert a closing force on the crack faces and shield the tip from the applied stress, which stops further crack propagation [21].

The effectiveness of this mechanism is governed by the binder properties, where more ductile binders can undergo more stretching before failure and therefore absorb more energy. Thicker binder ligaments, which are directly related to the binder mean free path, provide better resistance to rupture. The WC grain size plays an important role in ductile ligament bridging, since large WC grains lead to a larger mean free path for a constant binder volume fraction. [22].

### 2.3.3 Hardness-toughness dichotomy

Cemented carbides face an inherent limitation known as the hardness-toughness dichotomy. When the hardness increases by decreasing the WC grain size or the binder volume fraction, the fracture toughness decreases. Conversely, increasing the fracture toughness by increasing the binder volume fraction or WC grain size leads to a decrease in hardness. Cemented carbides with alternative binders, such as Fe-based alloys, offer the possibility of using the Transformation Induced Plasticity (TRIP) effect to overcome this constraint [23].

TRIP is fundamentally a deformation-induced mechanism where a material undergoes a phase transformation induced by plastic deformation. In Fe-based binders, the primary transformation responsible for the toughening associated with the TRIP effect is from metastable austenite with an FCC crystal structure into martensite, which has a BCC structure or BCT structure with lower carbon content. The transformation occurs through a diffusionless shear movement of atoms, which results in a crystallographic shape change and a volume expansion as the BCC structure is less dense than the FCC structure [5]. For the TRIP effect to be possible, the binder phase needs to exist in a metastable austenitic state at the cemented carbide's operating temperature. Another important factor is the carbon content in Fe-based alloys like the Fe-Ni-Co binder, since carbon is a potent austenite (FCC) stabilizer. High C-content in the binder would stabilize FCC and lower the martensitic transformation temperature, while a lower C-content would destabilize FCC and increase the martensitic transformation temperature ( $M_s$ ) [5][24][25]. This gives a final higher martensite fraction in the binder and increases the hardness. The inclusion of an austenite stabilizing element, like Ni, in the binder can help lower the martensitic transformation temperature ( $M_s$ ) and allow metastable austenite to remain in the structure at room temperature [5][26]. When the drill bit insert is deformed during

drilling, the induced mechanical stress is a driving force that is high enough for the metastable austenite to transform into martensite.

As the crack propagates through the material, the binder matrix surrounding the crack transforms into martensite. The primary toughening mechanism comes from the volume expansion of the martensite transformation. This local volume increase is hindered by the surrounding binder, which places a compressive stress ahead of and around the crack tip, shielding it from further propagation. [27] The key advantage of the TRIP effect in cemented carbides is that the bulk hardness of the material is unchanged while leveraging localized transformations within the structure to stop crack propagation and increase the toughness.

A study shows that hardness increases along with the Fe/Ni ratio in WC-Fe-Ni-Co. Indeed, this is due to Fe grain growth inhibition and its TRIP effect. It is shown that with a certain window ratio, the binder phase remains FCC shaped, but when the ratio continues to increase, the binder phase gradually changes to BCC, which significantly increases the hardness, until it reaches a second ratio window, when the structure is completely BCC shaped, and where hardness continues to increase, but slower. [4].

# 3 Experimental

## 3.1 Sample production and preparation

The four cemented carbide samples, each made of identical compositions but with varying ingoing WC raw material particle sizes, were produced in Sandvik Rock Tools' laboratory, in a rectangular shape, hypothetically without any concentration gradient. The samples were prepared for microstructure analysis and hardness testing in the Hultgren laboratory at KTH. To prepare the samples for the characterization tests, they were cut in half with a STRUERS Accutom-5 cutting machine equipped with a diamond wheel blade to expose the inner structure. The samples were then baked in bakelite with the cross section visible, to form a cylinder that could be mounted in the polishing machine. The samples were polished in a BUEHLER PowerPro 5000 polishing machine for 10 minutes at 150 RPM with a 9-micron polishing cloth with a 9-micron diamond solution, followed by 20 minutes with a 1-micron polishing cloth and a 1-micron diamond solution.

Once the samples were polished, they had obtained a mirror-like finish. Each sample was observed under a Light Optical Microscope (LOM) to look for scratches, which would determine if the samples needed further polishing. No visible scratches were found, and the LOM struggled to focus, which was a good indicator that the samples were properly polished.

It was concluded that the polishing process was sufficient, and to enhance the contrast between the different microstructural phases, the samples had to undergo an etching process. Half of the surface was covered with tape to protect it from the etching solution, while the other half was exposed to Murakami etchant, a potassium hexacyanoferrate(III) solution with 10% potassium hydroxide. To obtain satisfying pictures, the samples had to undergo different etching times. Samples 3, 4, and 5 got etched for a total of 70 seconds, and sample 2 got etched for 80 seconds.

Each step of the sample preparation process was preceded by a wash with ethanol in an ultrasonic cleaner.

## 3.2 Vickers hardness test

The hardness of the samples was measured using the Duramin-40 Microhardness Tester. The conditions were identical for each sample. The test was Vickers', with a charge of 20 kgf (giving HV20 unit of hardness), applied for 10 seconds. On each sample, 6 indents were made following the pattern visible in Figure 1. The indents were separated by 0,35 mm on the x axis and 0,70 mm on the y axis. The coordinates were chosen after an initial test indent, which helped determine how large the indents and cracks were, to avoid overlapping each other when doing the pattern indents.

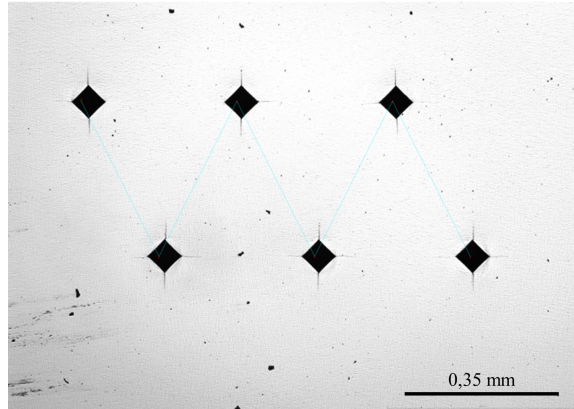


**Figure 1.** 6 indent pattern on sample 5

### 3.3 Fracture toughness

Fracture toughness quantifies a material's resistance to brittle fracture when a pre-existing flaw is present. It is one of the most important mechanical properties of cemented carbides and has great implications for rock drilling applications. The Palmqvist method is a common way of calculating the fracture toughness of cemented carbides. The fracture toughness is given by the stress intensity factor  $K_{IC}$  (MPa m<sup>1/2</sup>), where higher  $K_{IC}$  values indicate better crack propagation resistance. By using the length of the cracks from the Vickers hardness test, the fracture toughness is given by:

$$K_{IC} = 0,0028\sqrt{HV}\sqrt{\frac{P}{T}} \quad (1)$$

Where 0,0028 is an empirical constant, HV is the Vickers hardness in MPa, P is the indent load in N, and T is the total crack length in mm.

### 3.4 Light optical microscopy

The etched samples were observed at different magnifications in the LOM Olympus BX53M. Several snapshots of the microstructure are taken with a 20x, 50x, and 100x magnification. The pictures taken with the LOM on samples 2, 3, and 4 are used to calculate the average grain size of the WC, using the linear intercept method. For sample 5, the magnification wasn't sufficient to calculate the grain size with the linear intercept method.

### 3.5 Scanning electron microscopy

#### 3.5.1 Broad Ion Beam

Despite the 1 micron polishing the samples underwent, they were not polished enough for the Electron Backscatter Diffraction (EBSD). The samples were placed into a Jeol IB-19520CCP machine to undergo broad ion beam polishing. It removes residues from the mechanical polishing using an argon beam at a low angle in a vacuum chamber. [28]

### 3.5.2 Electron backscatter diffraction

The prepared samples were analyzed using a Nova 600 NanoLab FIB-SEM, equipped with an Oxford Instruments EBSD detector. In EBSD, a high-energy electron beam is directed onto the surface of the sample, which is tilted  $70^\circ$  relative to the incoming beam to optimize the diffraction conditions. Some electrons penetrate slightly into the material and are elastically scattered back out. As they exit, the electrons interact with the crystal lattice planes and form diffraction patterns, known as Kikuchi patterns, an example of which can be seen in Figure 2. These patterns are captured by the EBSD detector and analyzed using AZtec software. From the patterns, the system can determine properties such as crystal orientation and phase of the material. Grain size and shape can be obtained by post-processing the data from the EBSD.

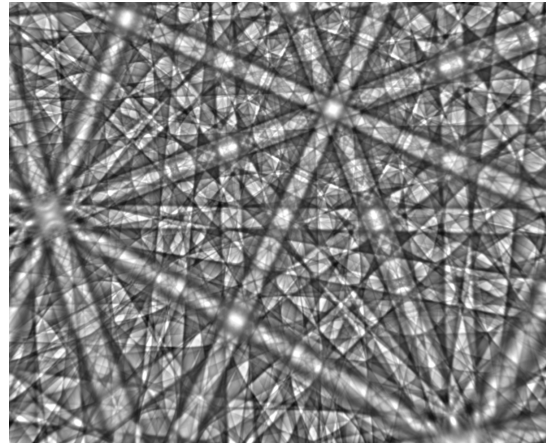


**Figure 2.** Experimental EBSD pattern from cubic  $ZrO_2$ . [29]

### 3.5.3 Post-processing EBSD data

The data obtained by the EBSD was post-processed with Matlab in combination with MTEX, which is an open-source Matlab toolbox made for analyzing and modeling crystallographic textures. When carrying out the processing, firstly, all the crystal symmetries are specified for the relevant phases that are present in the sample. Each of the phases was defined by its lattice parameters, phase name, and then assigned a unique color code for visualization. Thereafter, a grain reconstruction was made using a misorientation threshold of  $3^\circ$ , which allows for the identification of grain boundaries. Grains that were smaller than 3 pixels were excluded to reduce noise. Inverse pole figures (IPF) were also generated for each phase in the X-direction, which is used to illustrate the crystallographic orientation through color.

## 4 Results

### 4.1 Phase diagram

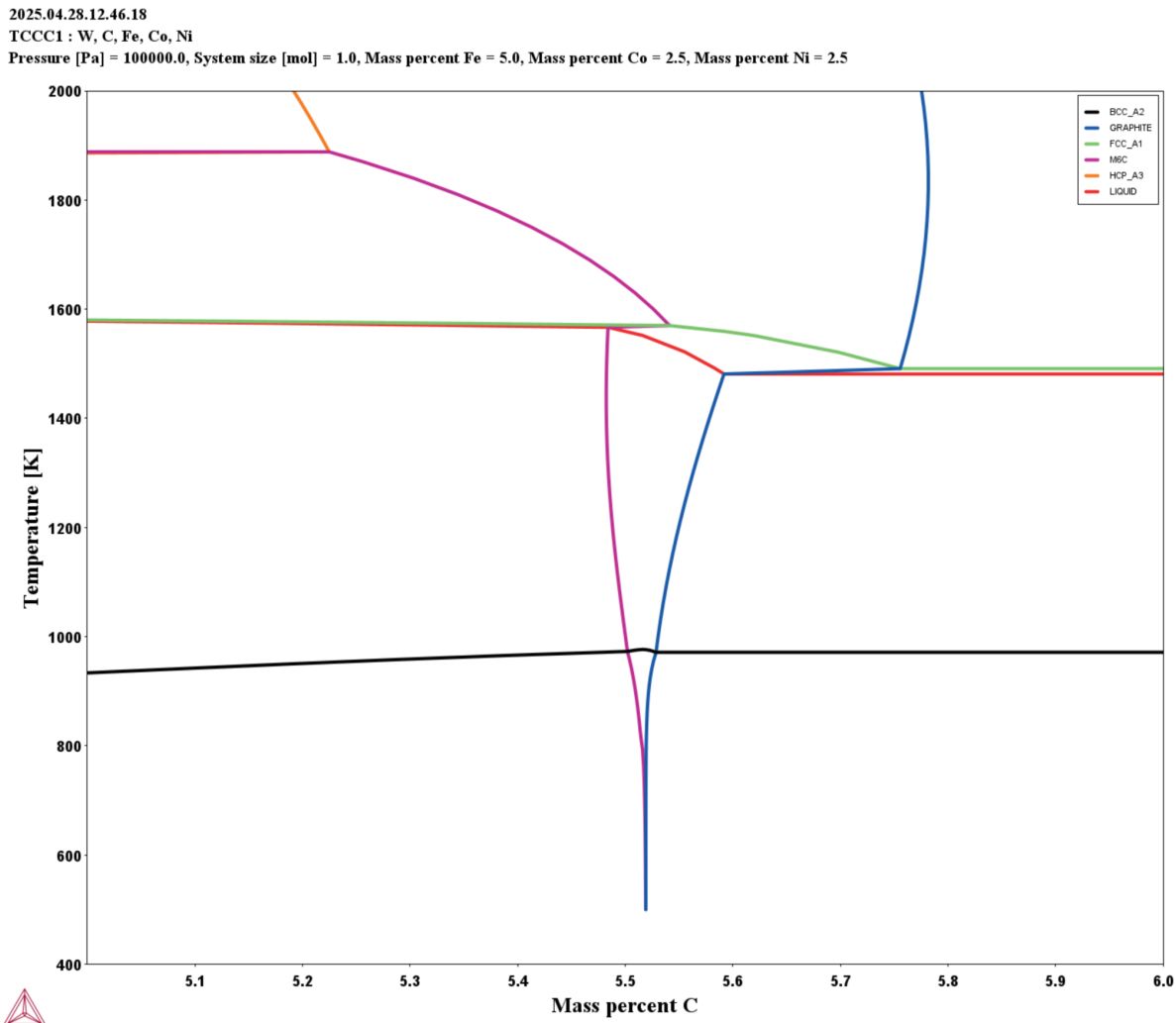


**Figure 3.** Phase diagram depending on carbon wt%, centered around the theoretical mass percent of carbon in the WC

A calculated phase diagram visible in figure 3 was generated via Thermo-Calc to understand the stability of different phases in the cemented carbide samples, depending on the carbon content. The diagram is centered around the theoretical carbon mass percentage for WC-based materials.

- HCP\_A3: a metallic HCP phase.
- FCC\_A1: represents the face-centered cubic structure of the Fe-Ni-Co metallic binder phase. The FCC structure is desirable as it contributes to improved toughness and ductility of the material.
- M6C: undesirable carbon-deficient  $\eta$ -phase.
- GRAPHITE: undesirable carbon-rich graphite phase.

- BCC\_A2: this phase corresponds to the body-centered cubic structure, most likely relating to a low-temperature form of the Fe-rich binder. The BCC phase is generally less ductile than FCC, and its presence could influence the mechanical properties negatively if not properly controlled.

WC phase, a hexagonal close-packed crystal structure of tungsten carbide, which is the primary hard phase providing hardness and wear resistance (commonly MC-SHP), is present everywhere on the diagram, so there are no lines for it on the present phase diagram.

## 4.2 Hardness

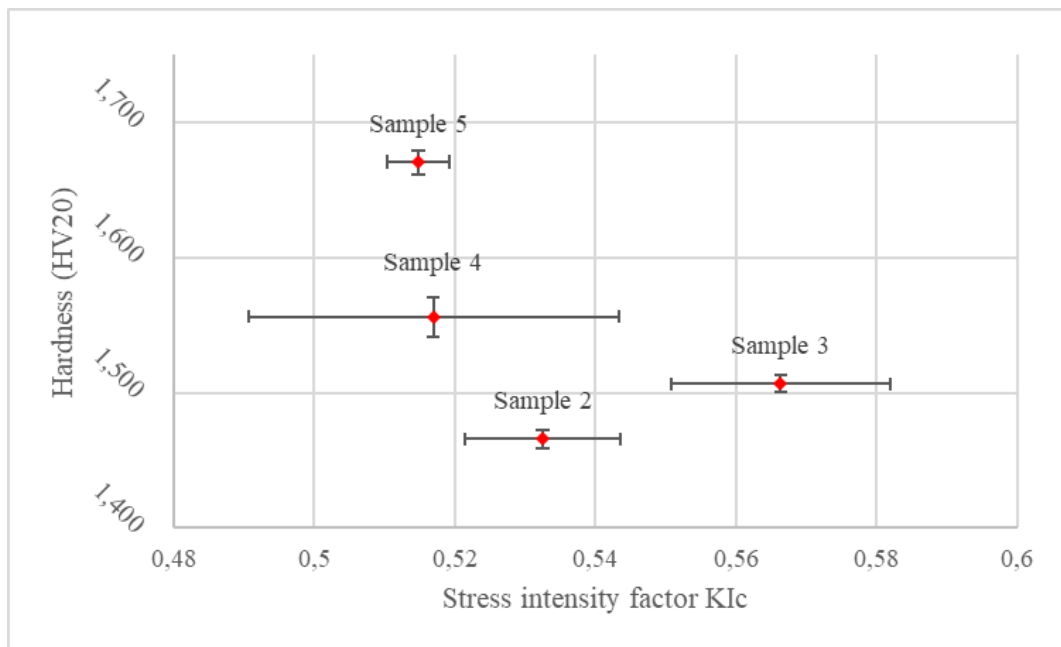


**Figure 4.** Hardness and fracture toughness of each sample

From Figure 4, it appears that the hardest sample is sample 5, then sample 4, sample 3, and finally sample 2. The standard deviation is calculated using the formula (2), see appendix A.

## 4.3 Fracture toughness

The fracture toughness calculations with the Palmqvist method implicitly depend on the specific mechanical properties and fracture behaviour of the WC-Co system. The empirical relationships established for WC-Co systems might not accurately describe the relationship between hardness, crack length, and fracture toughness in WC-Fe-Ni-Co systems. The Palmqvist method is also calibrated for HV30 values, and applying an HV20 value in the calculations violates the conditions under which the equation was derived. It is therefore not suitable to calculate the  $K_{IC}$  values of the samples with the Palmqvist method, as it is likely to produce unreliable results.

Despite not using the Palmqvist method, it is possible to compare the brittleness of the samples by calculating the total crack length of each sample from the Vickers hardness test, using the visible crack lengths on figures 5, 6, 7, and 8. Brittle materials have a lower fracture toughness and thereby longer total crack lengths.

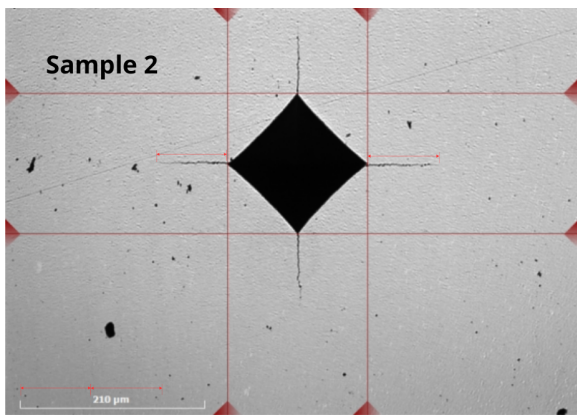


**Figure 5.** Sample 2 crack length

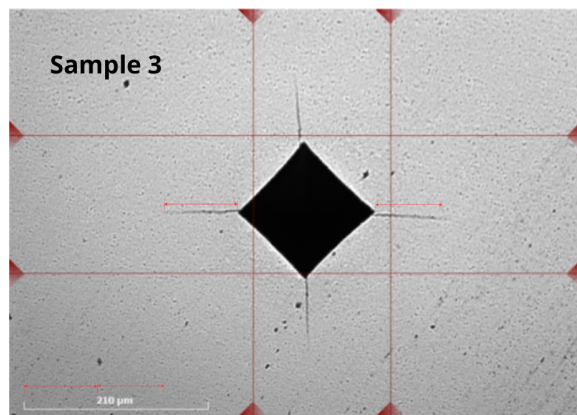


**Figure 6.** Sample 3 crack length

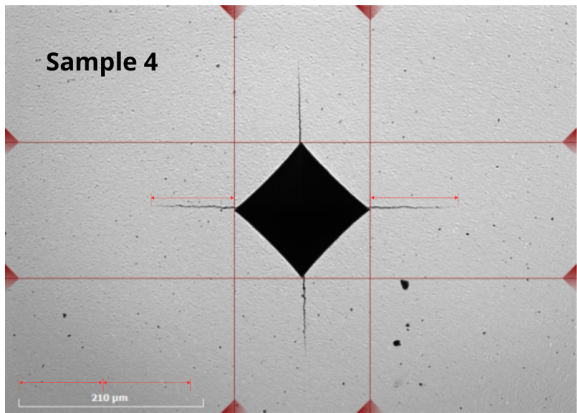


**Figure 7.** Sample 4 crack length

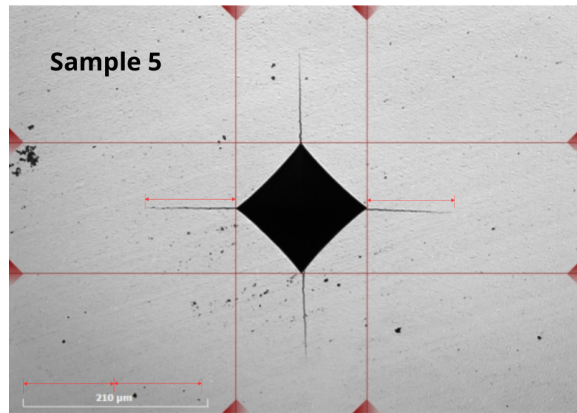


**Figure 8.** Sample 5 crack length

#### 4.4 Grain size

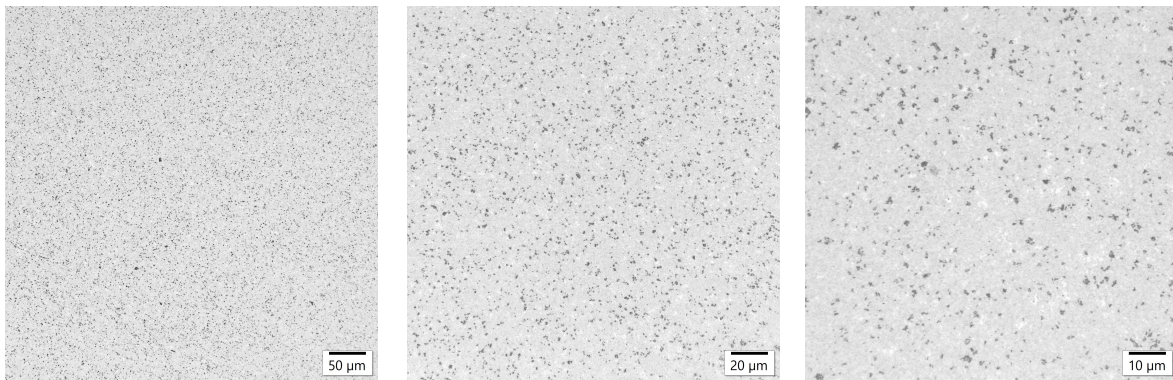


**Figure 9.** Pictures of sample 5 microstructure taken with 20x, 50x, and 100x magnification

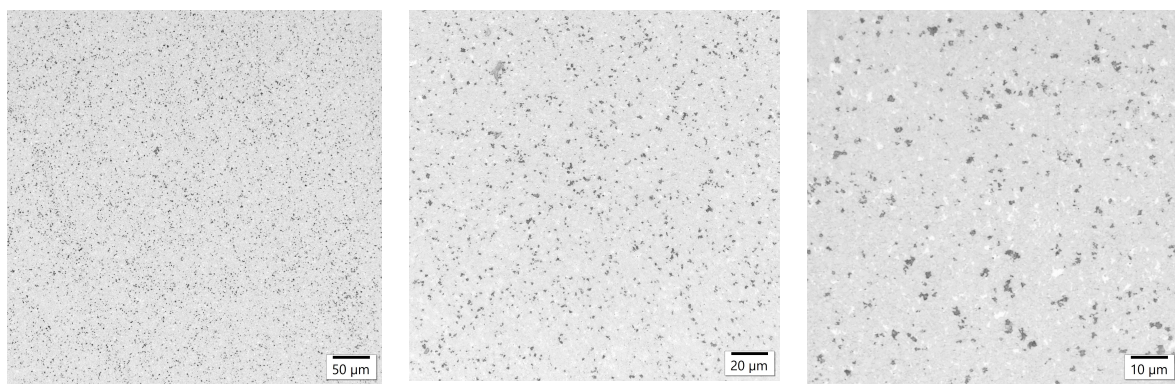


**Figure 10.** Pictures of sample 4 microstructure taken with 20x, 50x, and 100x magnification

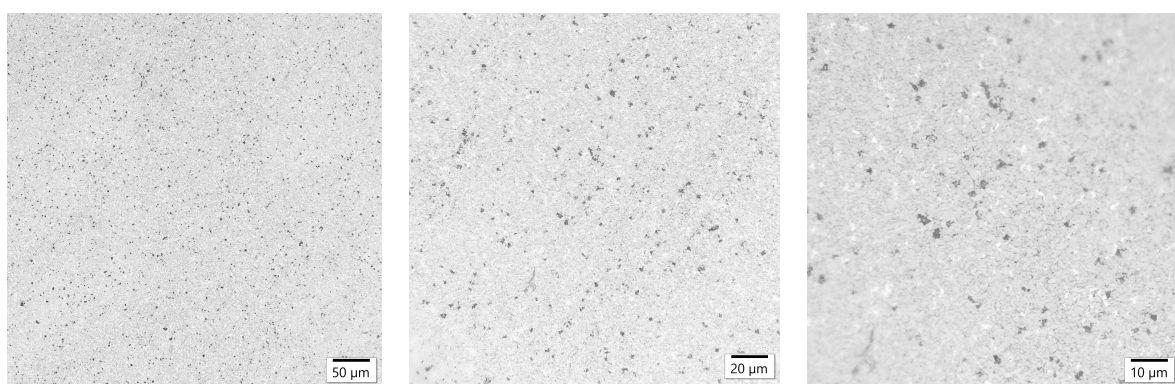


**Figure 11.** Pictures of sample 3 microstructure taken with 20x, 50x, and 100x magnification

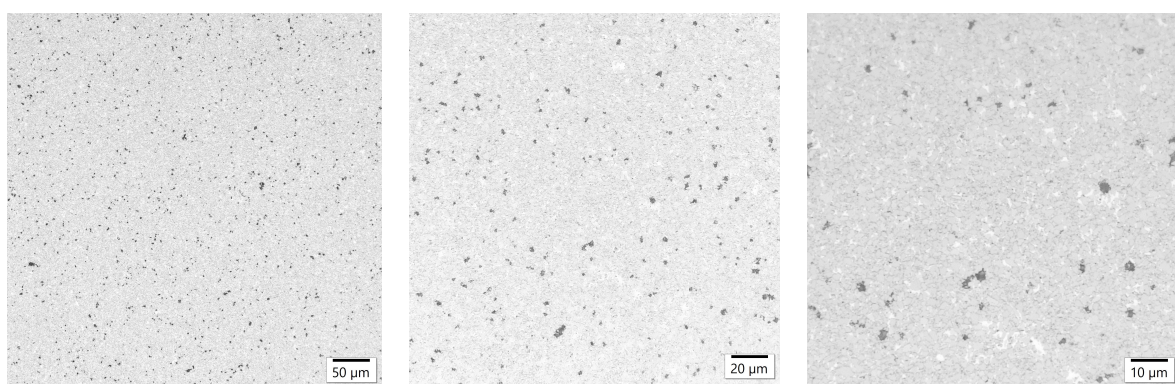


**Figure 12.** Pictures of sample 2 microstructure taken with 20x, 50x, and 100x magnification

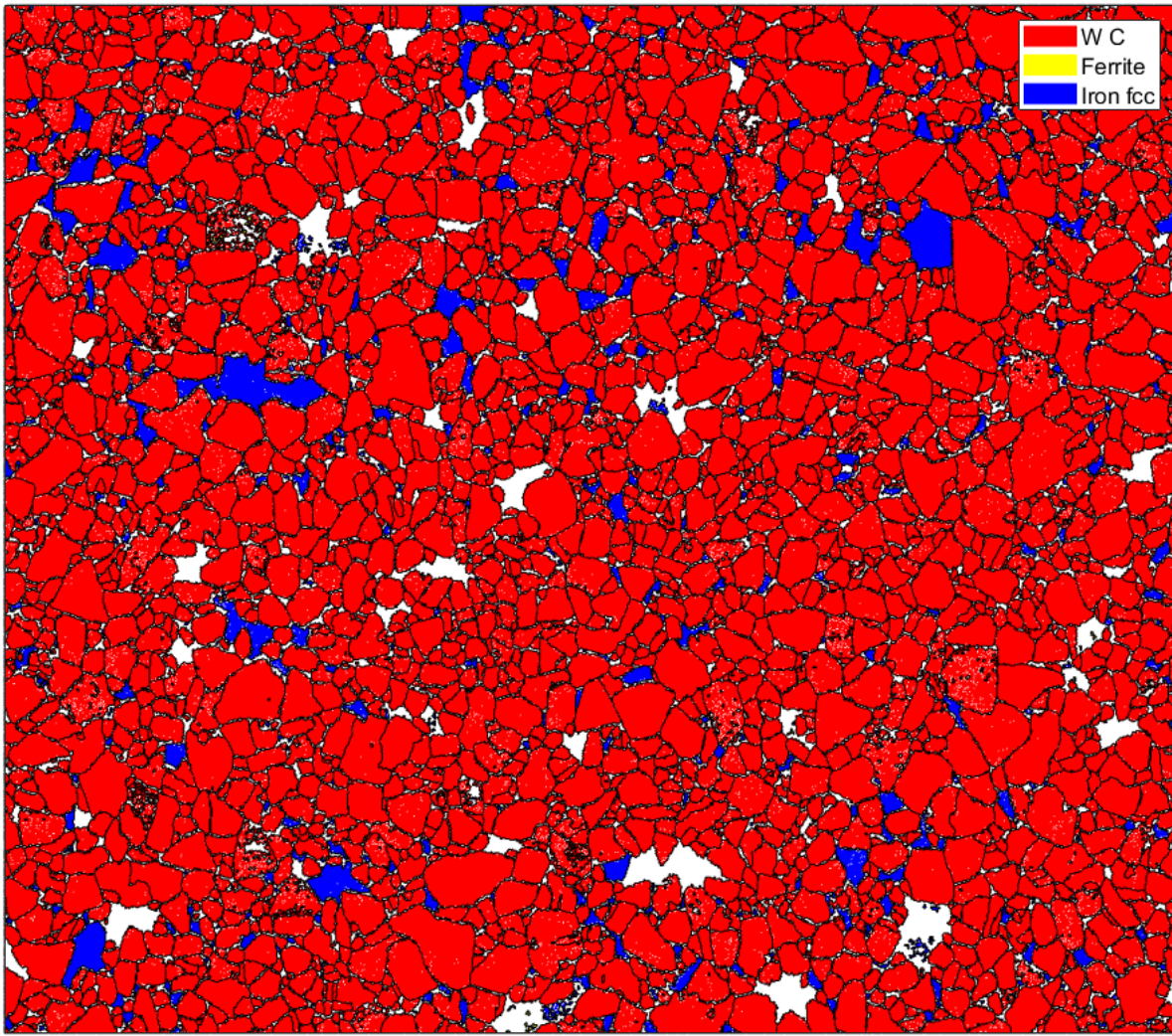


**Figure 13.** Phase plot of sample 5 with reconstructed grain boundaries from EBSD data at 20kV.

The average grain size of the samples was extracted using figures 9, 10, 11, and 12 with the linear intercept method, and using figure 13 with MTEX and Matlab calculations. The result was put in figure 14:

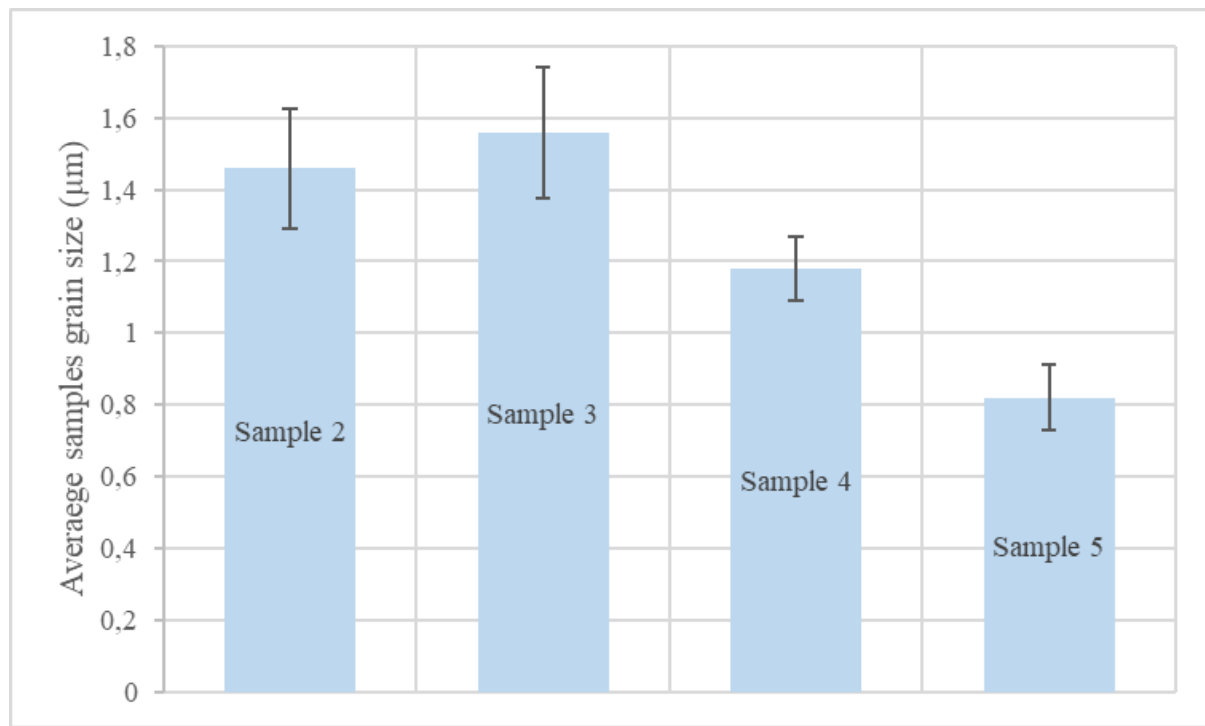


**Figure 14.** Average size of the grains

The results shown in figure 14, indicate that the average grain size was largest for sample 3, followed by sample 2 and sample 4, and lastly sample 5 with the smallest grain size.

All the obtained data from the results section are summarised in the following table 1:

**Table 1.** Summary of the mechanical properties of the samples

	Sample 2	Sample 3	Sample 4	Sample 5
Hardness (HV20)	1466	1507	1556	1671
Average total crack length ( $\mu\text{m}$ )	163,5	159	195	202,5
Average grain size ( $\mu\text{m}$ )	1,46	1,56	1,18	0,82

## 5 Discussion

### 5.1 Obtained results

The objective of this thesis is to investigate the mechanical properties of cemented carbide using an alternative binder to Co, being 50 wt% Fe, 25 wt% Ni, and 25 wt% Co. The focus has been on the effects of the initial WC powder grain sizes, which are different for each sample.

The Thermo-Calc calculated phase diagram indicates the presence of the WC phase, Fe-Ni-Co binder phase,  $\eta$ -phase, graphite, and a BCC Fe-rich phase. The presence of such phases must be validated by the EBSD data, which also indicates the amount of each phase. Also, there is another phase present in all samples, which appears as dark spots on LOM taken figures 9 to 12 and as non-indexed white areas on the EBSD map figure 13. These dark spots most closely resemble finely dispersed  $\eta$ -phase, which would indicate that the samples are slightly carbon deficient and further to the left in the phase diagram in figure 3. The presence of  $\eta$ -phase in cemented carbides increases the hardness but, conversely, negatively affects the fracture toughness [2].

From figure 4, hardness increases with the sample's number. On the other hand, the average crack length for the samples does not follow a monotonic trend, as sample 3 has the shortest crack length, while the other samples generally show increasing values. The grain size measurement indicates that sample 3 has the largest grains. Then, the grain size follows the same tendency as the crack length. It globally decreases with an increase for sample 3.

### 5.2 Discussion on hardness results

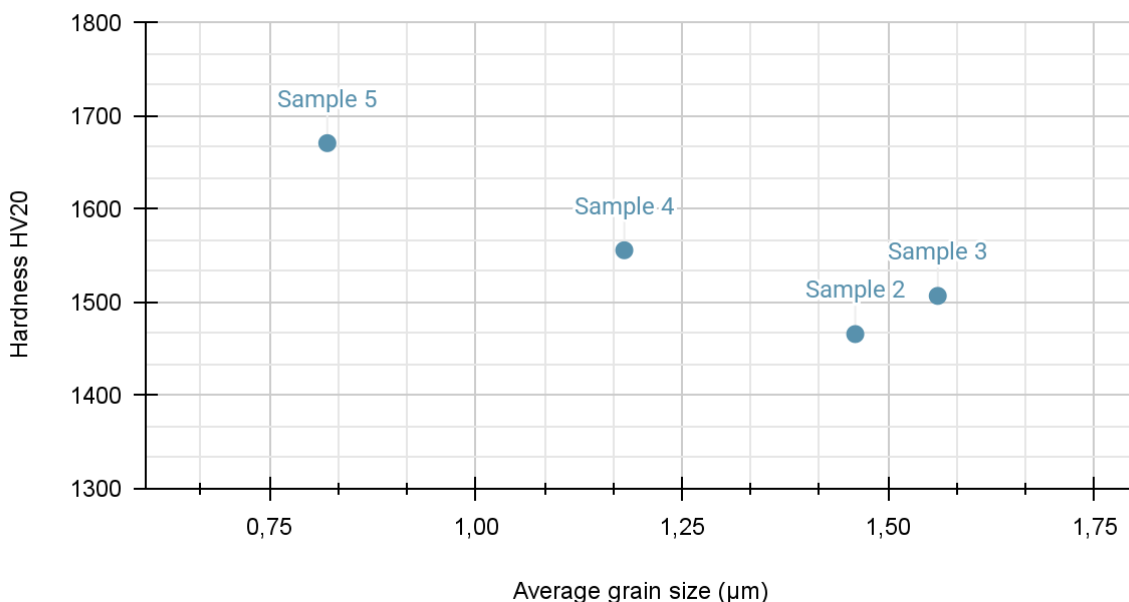


**Figure 15.** Hardness against average grain size

The increasing hardness trend seen in the samples corresponds well with the theory that a decrease in average grain size leads to an increase in hardness, which is visible in figure 15. This is also supported

by the Hall-Petch relationship, where a smaller grain size corresponds to a higher hardness. As the samples have the same binder volume fraction and composition, with the same manufacturing process and conditions, it can be argued that the ingoing WC raw material particle size plays a role in the final average grain size of the cemented carbides when an alternative Fe-Ni-Co alloy binder is used.

The literature supports that smaller ingoing WC raw material particles result in a finer grain size in the final microstructure [7]. Alternative binders with Fe in their composition also tend to result in smaller average grain sizes, due to the grain growth inhibiting properties of Fe [4]. Sample 5 has the highest hardness value and also the smallest average grain size of all the samples. The high hardness stems from the small average grain size, which in itself could be attributed to the samples' Fe-rich binders in combination with small WC raw material powder particles.

Sample 3 has a higher hardness than sample 2, yet the average grain size of sample 3 is larger than sample 2. This finding contradicts the idea that smaller grain sizes lead to higher hardness. One possible explanation could be that the Vickers hardness test for sample 3 was made in an area of the cemented carbide where trace amounts of  $\eta$ -phase were present. The presence of  $\eta$ -phase could locally increase the hardness, and if the indentations were made in one such area, it could affect the hardness value. With the same argument, sample 2 could have been indented in an area with trace amounts of graphite phase, which would have decreased the hardness locally. Since the LOM picture indicated the presence of  $\eta$ -phase, the theory of graphite can be neglected since the two phases can not exist at the same time. The indentations were intentionally placed in areas where the samples had no sign of  $\eta$ -phase. Since the indenter penetrates the samples, there could have been areas of  $\eta$ -phase present deeper in the microstructure that were not visible from the surface, which could have increased the hardness of sample 3. Albeit this argument, it would be unlikely that each of the six indentations would hit an area with  $\eta$ -phase.

Another explanation could be that sample 3 had larger initial WC powder particles than sample 2. This would, in theory, result in a larger average grain size for sample 3 but a lower hardness than sample 2. Fewer and larger initial WC powder particles would have a smaller total surface area, which could affect the rate or extent of carbon diffusion from WC to the binder during liquid sintering. This is due to fewer grain boundary areas where diffusion can take place. Less carbon diffusion would lead to a lower carbon content in the binder of Sample 3 compared to Sample 2. Since carbon is an effective austenite (FCC) stabilizer in Fe-based alloys like the Fe-Ni-Co binder, a lower carbon content in the binder would increase the martensitic transformation temperature ( $M_S$ ) as BCC would be more stable at room temperature [24][25]. This could result in a higher volume fraction of martensite in the binder of sample 3, which could increase the hardness of the cemented carbide even though the grain size is larger.

The most likely explanation for this contradiction is that the standard deviation bars in figure 14 show that sample 2 and 3 could have the same grain size, or even that sample 3 could have a smaller grain size than sample 2. The error is likely caused by inaccurate grain size measurements and not from the hardness measurement, which is likely correct. This would explain why sample 3 has a better hardness.

To compare hardness ranges, it is relevant to find WC-Co compositions that are similar to the one used for this thesis, which contain approximately 90 wt% of WC and 10 wt% of binder. The comparison is made with values from H. Engqvist, S. Jacobson and N. Axén [30] with similar

binder/WC compositions and various grain sizes. The following measures can be compared to the one calculated with Sandvik samples:

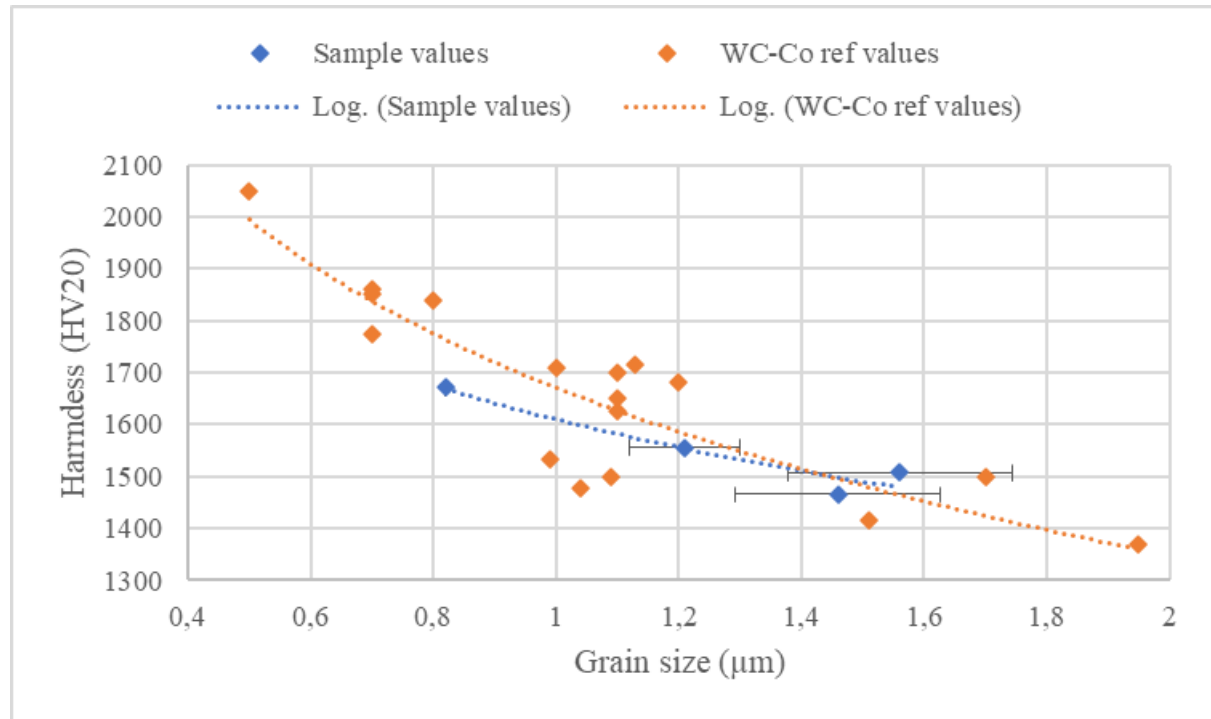


**Figure 16.** WC-Co hardness compared to WC-Fe-Ni-Co hardness

Looking at figure 16, logarithmic trend lines have been plotted for reference values and the Sandvik sample's values. These trends show that for the Sandvik samples, the hardness is decreasing more slowly than for the WC-Co values. Therefore, the hardness of the WC-Fe-Ni-Co is lower than the WC-Co for small grain size, and higher for large grain size. This means that the hardest cemented carbide would be a small grain size WC-Co material. As WC is used for high hardness applications, like rock milling, the WC-Co is better to use than the WC-Fe-Ni-Co.

However, this interpretation can be challenged due to the low number of data points for WC-Fe-Ni-Co. As the sample points are in the point cloud, the difference between WC-Co and WC-Fe-Ni-Co hardness is not significant, and could be negligible. Moreover, this analysis only considers hardness, and not toughness, which is necessary for maximized durability and efficiency of the material, and that is promoted by the presence of Fe in WC-Fe-Ni-Co.

As Fe is a grain growth inhibitor, the more Fe there is in the binder, the smaller are the grains and the higher the hardness is. Also, the higher the Fe/Ni ratio, the harder the WC is. Then, compared to other WC-Fe-Ni-Co, some with a higher Fe/Ni ratio in the binder (higher than 2) would be harder. And some with lower ratios would get lower. [4]

### 5.3 Discussion of crack length and fracture toughness

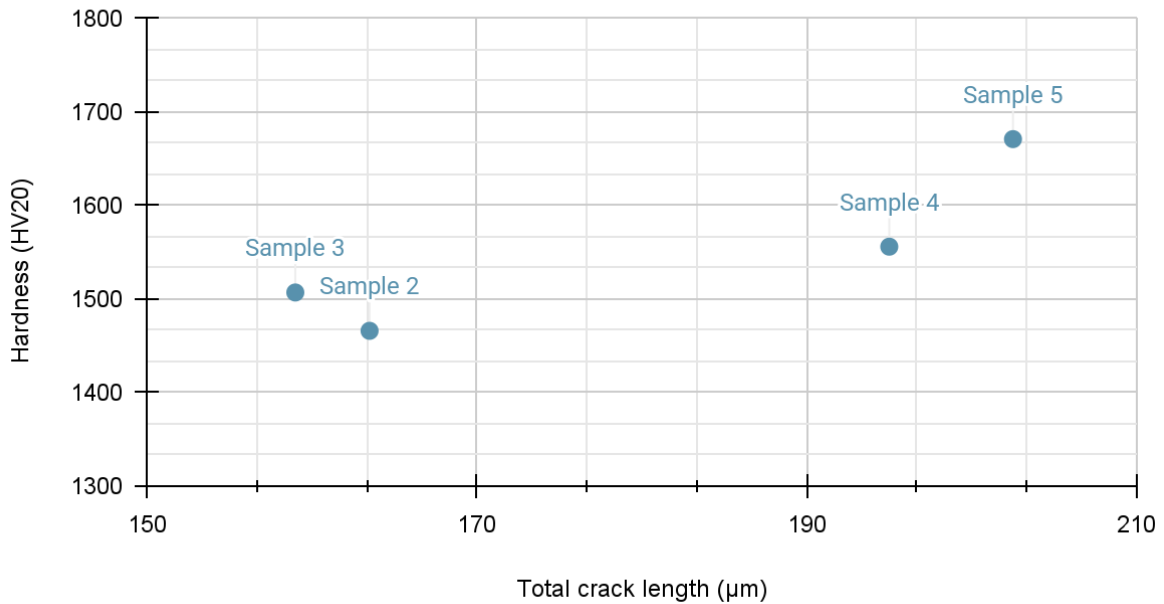


**Figure 17.** Hardness against total crack length

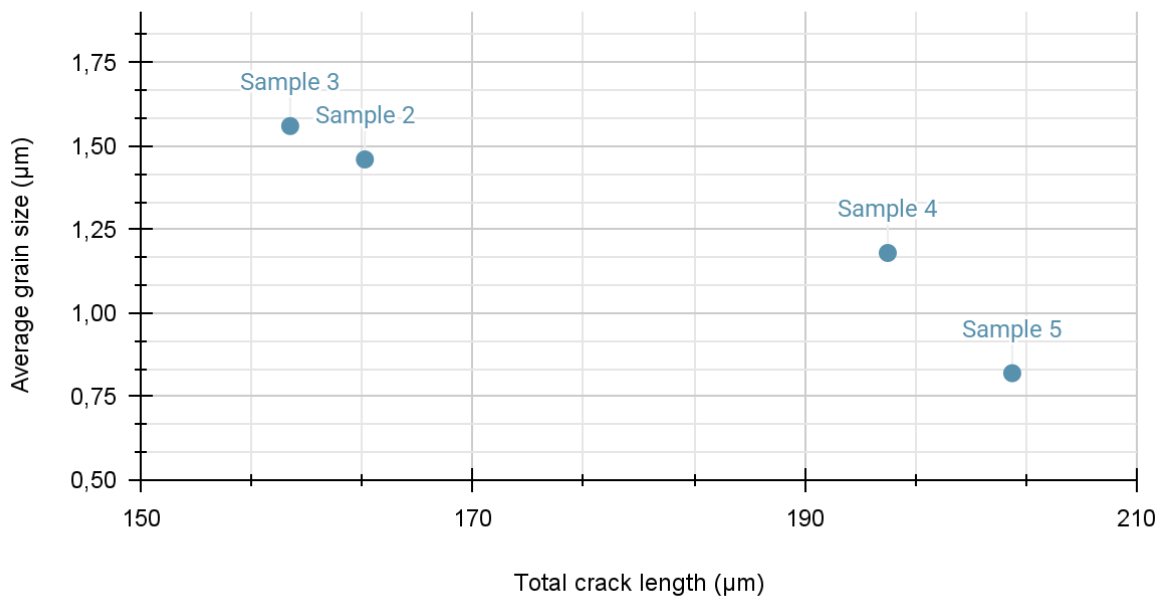


**Figure 18.** Average grain size against total crack length

The total crack length increases in sample 3 to 5 but decreases from sample 2 to 3, which can give an indication of the samples' fracture toughness. Although the Palmqvist method was deemed unusable for our samples due to their alternative Fe-Ni-Co binder and the hardness calculations using HV20 (whereas the Palmqvist formula for calculating  $K_{\text{IC}}$  is calibrated for Co-binders and HV30 values), the total crack length can still show how well the samples can resist the propagation of cracks.

From figure 17, it is deductible that sample 5 has the longest crack length as well as the highest hardness, which correlates well with the expected hardness-toughness trade-off, where increasing

hardness comes at the expense of a lower fracture toughness. This can also be seen in figure 18, where a smaller average grain size leads to a longer total crack length, which can be attributed to crack deflection [18]. When a crack propagates through the material and runs into a hard WC grain, it is more energy efficient for it to deflect and propagate around the WC grain. When the crack runs into larger WC grains, it has to travel a longer distance, which requires a higher energy input and thereby increases the fracture toughness. Sample 5 has smaller grains, which are easier for the crack to propagate around, and hence it has a longer total crack length than the other samples with larger grains.

In Figure 18, it can be observed that sample 3 has a shorter total crack length than sample 2, which deviates from the theoretical assumption that toughness decreases when grain size increases. It could be explained by the hardness test done on a mostly undesirable cross section ( $\eta$ -phase or graphite), but most likely because of measurement inaccuracies of the average grain size. Samples 2 and 3 have similar grain sizes, and as mentioned, it can be seen in figure 14 that the standard deviation suggests that sample 2 could have a larger average grain size than sample 3, which would explain the shorter total crack length.

It is difficult to compare the toughness of the WC-Fe-Ni-Co samples with the WC-Co from the literature as the  $K_{IC}$  cannot be calculated for the present samples. But, it is possible to backtrack the Palmqvist method and obtain the average crack length with equation (1) for other cemented carbide grades like the one from F.L. Zhang, M. Zhu, C.Y. Wang [15]. Only a part of their data was used for the comparison: measures that were taken with HV30, on samples with a binder ratio of approximately 10%, which is comparable to the quantity of binder in the present samples.

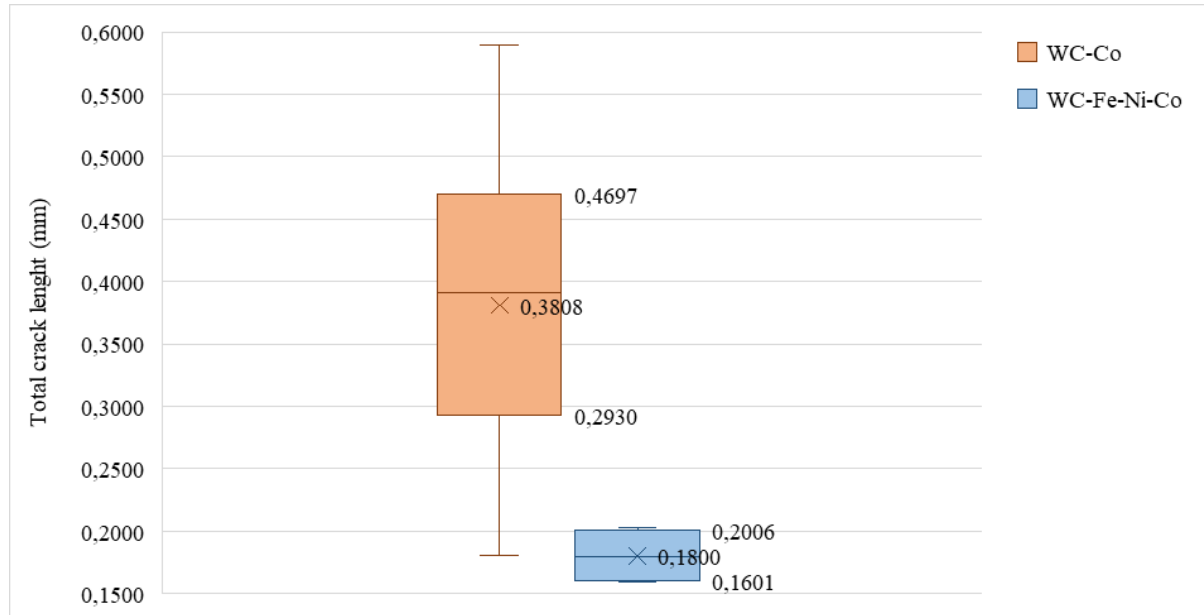


**Figure 19.** Box plot of the crack length for WC-Co and for the WC-Fe-Ni-Co samples

From figure 19, it appears that the WC-Co has a bigger crack length than WC-Fe-Ni-Co, which indicates that they have a lower toughness, and are probably harder.

But, the values can be discussed as WC-Co endured an HV30 test, which uses a bigger force on the sample than the HV20 that was done on the present samples. A bigger force logically results in bigger

cracks. Moreover, the WC-Co benefits from 50 measurements, while the present samples only have 4 measurements, which gives less precise and complete information.

## 5.4 Sources of errors

An insufficient number of measurements could be a source of error, particularly for fracture toughness, which was calculated with only a single total crack length measurement for each sample. More crack length measurements at different Vickers hardness test loads would give a more accurate comparison of fracture toughness between different specimens.

The linear intercept and crack length measurements were taken by hand. This can result in subjective data that varies depending on who took it. Also, the linear intercept can be calculated with too short intercepts, giving grain sizes that are not accurate enough to be an average size. This gives approximate data for grain size and comparison of samples.

Images taken by the LOM can be blurred due to less than ideal conditions, the table not being stable enough, and moving with the LOM when touched. It contributes to the approximation of the grain size measurements.

The phase diagram was made without knowing the exact composition of the samples, using approximate percentages of components, giving an approximate carbon composition and temperature.

A possible source of error during the EBSD measurements was vibrations in the building. Small vibrations can slightly move the sample or distort the electron beam, which can lead to blurrier images or less sharp Kikuchi patterns. This could have affected the outcome of the EBSD data. Factors like these are difficult to fully control and should be considered when evaluating the quality and accuracy of the microscopy results.

## 5.5 Social and ethical aspects

One of the reasons for exploring alternative binders for cemented carbides, like the Fe-Ni-Co system, which is studied in this work, is to address the ethical and environmental concerns that are linked to cobalt usage. A large part of the world's cobalt supply comes from regions where mining is associated with poor working conditions, child labor, and serious environmental damage. Reducing the amount of cobalt needed in industrial applications could help decrease the demand and lessen the social problems that are connected to its extraction.

Even though the Fe-Ni-Co binder still contains cobalt, using less of it is a step in the right direction. However, it's also important to remember that the mining and processing of iron and nickel have their own environmental impacts. In the future, more research could look not only at the mechanical performance of new binders but also at their overall sustainability, from raw material extraction to recycling possibilities.

## 6 Conclusions

Cemented carbides with alternative Fe-Ni-Co binders seem to follow the same trend as traditional Co-based binders, with increasing hardness as a result of decreasing the average grain size. The deviation from this trend between samples 2 and 3 can most likely be attributed to inaccurate measurements. It could be investigated further and more accurately with EBSD analysis of all four samples.

The trade-off between hardness and toughness continues to be a challenge when designing cemented carbides with alternative Fe-Ni-Co binders. Smaller initial WC powder particles result in a decrease in the average grain size, which leads to an increase in hardness. Increased hardness comes at the expense of fracture toughness, where smaller grain sizes decrease the fracture toughness due to the restricted crack deflection ability. Larger grains present higher barriers for planar crack propagation and are therefore more effective at increasing fracture toughness. However, this weakness for fine-grain cemented carbides could be mitigated with the TRIP effect, which is especially relevant for binders with austenite-stabilizing alloying elements, such as Ni.

An interesting possible finding when using larger initial WC powder particles in Fe-Ni-Co binders is the austenite (FCC) stabilizing effect of carbon in Fe-based alloys. For a constant volume fraction, large WC particles have less total surface area than smaller particles, which lowers the rate of diffusion from WC to the binder and decreases the carbon content in the binder. Due to carbon's austenite (FCC) stabilizing effects, a low carbon binder is more likely to have a higher fraction of martensite (BCC) at room temperature. This could suggest that larger initial WC powder particles could result in a cemented carbide with higher hardness while having larger average grain sizes. As a consequence, the fracture toughness would be a concern due to the brittleness of martensite, and it can be argued that the small increase in hardness from using larger WC powder particles is not worth the decrease in fracture toughness. Although Figure 19 shows a large decrease in total crack length for cemented carbides with an Fe-Ni-Co binder compared to a Co-based binder, one has to take into consideration that the total crack length depends on the load that was used for the hardness test. Further testing needs to be conducted to get a better understanding of the fracture toughness of Fe-Ni-Co-based cemented carbides when different initial WC powder particle sizes are used.

## 7 Future work

To better understand the potential of Fe-Ni-Co as a sustainable binder in cemented carbides, future work could explore a broader range of WC grain sizes and try different ratios of iron, nickel, and cobalt. This would give a clearer picture of how the microstructure affects the materials' properties and help to optimize the binder composition for specific applications. It would also be valuable to take a deeper look at the microstructure using more advanced EBSD analysis. This would allow for a more detailed understanding of how microstructural features such as grain orientation and misorientation affect mechanical behavior.

## 8 Acknowledgment

We, the authors, Simon Bonn, Axel Magnusson, and Rose Cuvillon, would like to thank our supervisor, Lisa Toller-Nordström, for her engagement and guidance during the project, and for assisting and conducting the experiments. We would also like to thank our supervisors at Sandvik Mining & Rock Solutions, Stella Sten and Ida Borgh, for giving us the opportunity to write our thesis for Sandvik and providing the WC samples.

## 9 References

- [1] Cobalt Institute, Cobalt 2050: Unlocking potential for a net-zero future, Cobalt Institute, 2024. Available:[https://www.cobaltinstitute.org/wp-content/uploads/2024/10/Cobalt-2050\\_Unlocking-potential-for-a-net-zero-future.pdf](https://www.cobaltinstitute.org/wp-content/uploads/2024/10/Cobalt-2050_Unlocking-potential-for-a-net-zero-future.pdf) [Accessed 20 February 2025]
- [2] García J., Collado Ciprés V., Blomqvist A., & Kaplan B, Cemented carbide microstructures: A review. International Journal of Refractory Metals and Hard Materials, vol. 80, pp. 40-68, 2019. Available: <https://doi.org/10.1016/j.ijrmhm.2018.12.004> [Accessed 17 February 2025]
- [3] Xiang, Z., Li, Z., Chang, F., & Dai, P. (2019). Effect of Heat Treatment on the Microstructure and Properties of Ultrafine WC-Co Cemented Carbide. *Metals*, 9(12), 1302. Available: <https://doi.org/10.3390/met9121302> [Accessed 26 April 2025]
- [4] Gao, Y., Luo, B., He, K., Zhang, W., & Bai, Z. (2018). Effect of Fe/Ni ratio on the microstructure and properties of WC-Fe-Ni-Co cemented carbides. *Ceramics International*, 44(2), 2030-2041. Available: <https://doi.org/10.1016/j.ceramint.2017.10.148> [Accessed 27 April 2025]
- [5] Liu, C. (2014). Alternative binder phases for WC cemented carbides (Dissertation). Available: <https://urn.kb.se/resolve?urn=urn:nbn:se:kth:diva-168229> [Accessed 28 April 2025]
- [6] Xu, K., Wang, Z., Cao, P., Peng, X., Chen, C., Liu, Q., Xie, S., Wu, X., & Jian, Y. (2024). Microstructure, Mechanical Properties and Wear Behaviors of Ultrafine-Grain WC-Based Cermets with Different Binder Phases Fabricated by Spark Plasma Sintering. *Materials*, 17(3), 659. Available: <https://doi.org/10.3390/ma17030659> [Accessed 28 April 2025]
- [7] Sun, Y., Su, W., Yang, H., & Ruan, J. (2015). Effects of WC particle size on sintering behavior and mechanical properties of coarse grained WC-8Co cemented carbides fabricated by unmilled composite powders. *Ceramics International*, 41(10), 14482-14491. Available: <https://doi.org/10.1016/j.ceramint.2015.07.086> [Accessed 28 April 2025]
- [8] T. Perrin, S. Achache, P-J. Meausoone, F. Sanchette, Characterization of WC-doped NiCrBSi coatings deposited by Laser Cladding; effects of particle size and content of WC powder, Surface and Coatings Technology, vol. 425, 2021, Available: <https://doi.org/10.1016/j.surfcoat.2021.127703> [Accessed 17 April 2025]
- [9] Roebuck B., & Bennett E., Phase size distribution in WC/Co hardmetal, Metallography, vol. 19, issue 1, pp. 27-47, 1986. Available: [https://doi.org/10.1016/0026-0800\(86\)90005-4](https://doi.org/10.1016/0026-0800(86)90005-4) [Accessed 11 March 2025]
- [10] Golovchan V., & Litoshenko N., On the contiguity of carbide phase in WC-Co hardmetals, International Journal of Refractory Metals and Hard Materials, vol. 21, issue 5-6, pp. 241-244, 2003. Available: [https://doi.org/10.1016/S0263-4368\(03\)00047-7](https://doi.org/10.1016/S0263-4368(03)00047-7) [Accesses 11 March 2025]
- [11] Kim, C.-S. (n.d.). Microstructural-Mechanical Property Relationships in WC-Co composites (By Materials Science and Engineering Department, Carnegie Mellon University). Available: [http://mimp.materials.cmu.edu/~gr20/theses/Kim\\_thesis.pdf](http://mimp.materials.cmu.edu/~gr20/theses/Kim_thesis.pdf) [Accessed 24 April 2025]

- [12] Gu L., Huang J., & Xie C., Effects of carbon content on microstructure and properties of WC–20Co cemented carbides, International Journal of Refractory Metals and Hard Materials, vol. 42, pp. 228-232, 2013. Available: <https://doi.org/10.1016/j.ijrmhm.2013.09.010> [Accessed 3 March 2025]
- [13] Qian, C., Liu, Y., Cheng, H., Li, K., Liu, B., & Zhang, X. (2022). The Effect of Carbon Content on the Microstructure and Mechanical Properties of Cemented Carbides with a CoNiFeCr High Entropy Alloy Binder. *Materials*, 15(16), 5780. Available: <https://doi.org/10.3390/ma15165780> [Accessed 28 April 2025]
- [14] Hillert M., Ågren J. & Borgenstam A., Mikro och nanostrukturer i materialdesign, Stockholm: Institutionen för Materialvetenskap, Kungliga Tekniska Högskolan, 2005. LIBRIS-ID:11936409
- [15] F.L. Zhang, M. Zhu, C.Y. Wang, Parameters optimization in the planetary ball milling of nanostructured tungsten carbide/cobalt powder, International Journal of Refractory Metals and Hard Materials, vol. 26, issue 4, pp. 329-33, 2008, Available: <https://doi.org/10.1016/j.ijrmhm.2007.08.005> [Accessed 18 March 2025]
- [16] Chychko, A., García, J., Collado Ciprés, V., Holmström, E., & Blomqvist, A. (2022). HV-KIC property charts of cemented carbides: A comprehensive data collection. *International Journal of Refractory Metals and Hard Materials*, 103, 105763. Available: <https://doi.org/10.1016/j.ijrmhm.2021.105763> [Accessed 28 April 2025]
- [17] Siwak, P. (2021). Indentation Induced Mechanical Behavior of Spark Plasma Sintered WC-Co Cemented Carbides Alloyed with Cr<sub>3</sub>C<sub>2</sub>, TaC-NbC, TiC, and VC. *Materials*, 14(1), 217. Available: <https://doi.org/10.3390/ma14010217> [Accessed 28 April 2025]
- [18] Roebuck, B., Bennett Eric., Lay, Lewis., Morrell, Roger., (2008) Measurement Good Practice Guide No. 9 Palmqvist Toughness for Hard and Brittle Materials. *Centre for Materials Measurement and Technology National Physical Laboratory*. Available: <https://eprintspublications.npl.co.uk/1566/1/mgpg9.pdf> [Accessed 28 April 2025]
- [19] Tarragó, J., Roa, J., Valle, V., Marshall, J., & Llanes, L. (2015). Fracture and fatigue behavior of WC–Co and WC–CoNi cemented carbides. *International Journal of Refractory Metals and Hard Materials*, 49, 184-191. Available: <https://doi.org/10.1016/j.ijrmhm.2014.07.027> [Accessed 28 April 2025]
- [20] Llanes, L. (2019). In-Depth Understanding of Fatigue Micromechanisms in Cemented Carbides: Implications for Optimal Microstructural Tailoring. *Metals*, 9(9), 924. Available: <https://doi.org/10.3390/met9090924> [Accessed 28 April 2025]
- [21] Tarragó, J. M. (2016). Damage tolerance of cemented carbides under service-like conditions. In Department of Materials Science and Metallurgical Engineering [Thesis]. Available: <https://www.tdx.cat/bitstream/handle/10803/403888/TJMTC1de1.pdf?sequence=1&isAllowed=y> [Accessed 27 April 2025]
- [22] Llanes, L., Torres, Y., & Anglada, M. (2002). On the fatigue crack growth behavior of WC–Co cemented carbides: Kinetics description, microstructural effects and fatigue sensitivity. *Acta Materialia*, 50(9), 2381-2393. Available: [https://doi.org/10.1016/S1359-6454\(02\)00071-X](https://doi.org/10.1016/S1359-6454(02)00071-X) [Accessed 27 April 2025]

- [23] Toller-Nordström, L., Sten, S., Kritikos, M., Norgren, S., Borgenstam, A., & Borgh, I. (2025). Wear properties of cemented carbides with new binder solutions for rock drilling inserts. *Wear*, 205909. Available: <https://doi.org/10.1016/j.wear.2025.205909> [Accessed 1 May 2025]
- [24] Saenarjhan, N., Kang, J., & Kim, S. (2019). Effects of carbon and nitrogen on austenite stability and tensile deformation behavior of 15Cr-15Mn-4Ni based austenitic stainless steels. *Materials Science and Engineering: A*, 742, 608-616. Available: <https://doi.org/10.1016/j.msea.2018.11.048> [Accessed 5 May 2025]
- [25] Stormvinter, A., Miyamoto, G., Furuhashi, T., Hedström, P., & Borgenstam, A. (2012). Effect of carbon content on variant pairing of martensite in Fe-C alloys. *Acta Materialia*, 60(20), 7265-7274. Available: <https://doi.org/10.1016/j.actamat.2012.09.046> [Accessed 5 May 2025]
- [26] Toller-Nordström, L. (2019). Insights into wear and deformation of alternative binder hardmetals. Digital Comprehensive Summaries of Uppsala Dissertations from the Faculty of Science and Technology 1873. 77 pp. Uppsala: Acta Universitatis Upsaliensis. ISBN 978-91-513-0789-3 Available: <https://www.diva-portal.org/smash/get/diva2:1362889/FULLTEXT01.pdf> [Accessed 1 May 2025]
- [27] C.Y. Huo, H.L. Gao (2005). Strain-induced martensitic transformation in fatigue crack tip zone for a high strength steel. Materials Characterization. Volume 55, Issue 1. Pages 12-18. ISSN 1044-5803. Available: <https://doi.org/10.1016/j.matchar.2005.02.004> [Accessed 1 May 2025]
- [28] Jeol, IB-19520CCP CROSS SECTION POLISHER™, Jeol, Available: <https://www.jeol.com/products/scientific/cp/IB-19520CCP.php> [Accessed 24 April 2025]
- [29] EDAX, *Left – Experimental EBSD pattern from cubic ZrO<sub>2</sub>*, EBSD Explained, EDAX. Available: <https://www.ebsd.com/ebsd-explained/pattern-formation> [Accessed 28 April 2025]
- [30] H. Engqvist, S. Jacobson, N. Axén, A model for the hardness of cemented carbides, *Wear*, vol. 252, issues 5–6, pp. 384-393, 2002, Available: [https://doi.org/10.1016/S0043-1648\(01\)00866-3](https://doi.org/10.1016/S0043-1648(01)00866-3) [Accessed 2 May 2025]

# Appendix

## A) Fracture toughness

$$K_{Ic} = 0,0028\sqrt{HV}\sqrt{\frac{P}{T}} \quad (1)$$

Where 0,0028 is an empirical constant, HV is the Vickers hardness in MPa, P is the indent load in N, and T is the total crack length in mm.

## B) Standard deviation $\sigma$ , calculated for the hardness and fracture toughness:

$$\sigma = \sqrt{\frac{\sum(x - \bar{x})^2}{n-1}} \quad (2)$$

Where  $x$  corresponds to each value of hardness or stress intensity factor  $K_{IC}$  measured,  $\bar{x}$  is the average of all these values, and n is the number of values.

## C) Calculated values for $K_{IC}$ against hardness plot

*Table 2. values calculated for figure 4*

$K_{IC}$ (-)	Hardness (HV20)	Standard deviation for $K_{IC}$	Standard deviation for hardness
0,5325	1,466	0,01104	0,0065
0,56632	1,507	0,01558	0,0064
0,51695	1,556	0,02631	0,0147
0,51481	1,671	0,00440	0,0089

The hardness values are reused for figure 15 and 17.

D) Grain size measures taken with linear intercept method

*Table 3. linear intercepts measures used for figure 14*

	Sample 2	Sample 3	Sample 4
Grain size measurements ( $\mu\text{m}$ )	1,404	1,726	1,36
	1,858	1,683	1,40
	1,602	1,693	1,23
	1,55	1,587	1,18
	1,558	1,588	1,18
	1,428	1,44	1,29
	1,35	1,4	1,09
	1,23	1,28	1,16
	1,29	1,36	1,20
	1,38	1,33	1,07
	1,25	1,3	1,13
	1,19	1,37	1,18
	1,61	1,72	1,10
	1,51	1,76	1,20
	1,56	1,67	1,13
	1,35	1,61	1,11
	1,51	1,72	1,20
	1,56	1,85	1,12
Average ( $\mu\text{m}$ )	1,46	1,56	1,18
Standard deviation	0,167	0,183	0,09

These grain size measures are reused for figure 15 and 18.

E) Grain size measurement with Matlab (sample 5)

Measures were made in Matlab with the EBSD data. About 1000 grains were measured and grain size determined with the equations below. Full code and all post-processing pictures can be found in this [github repository](#).

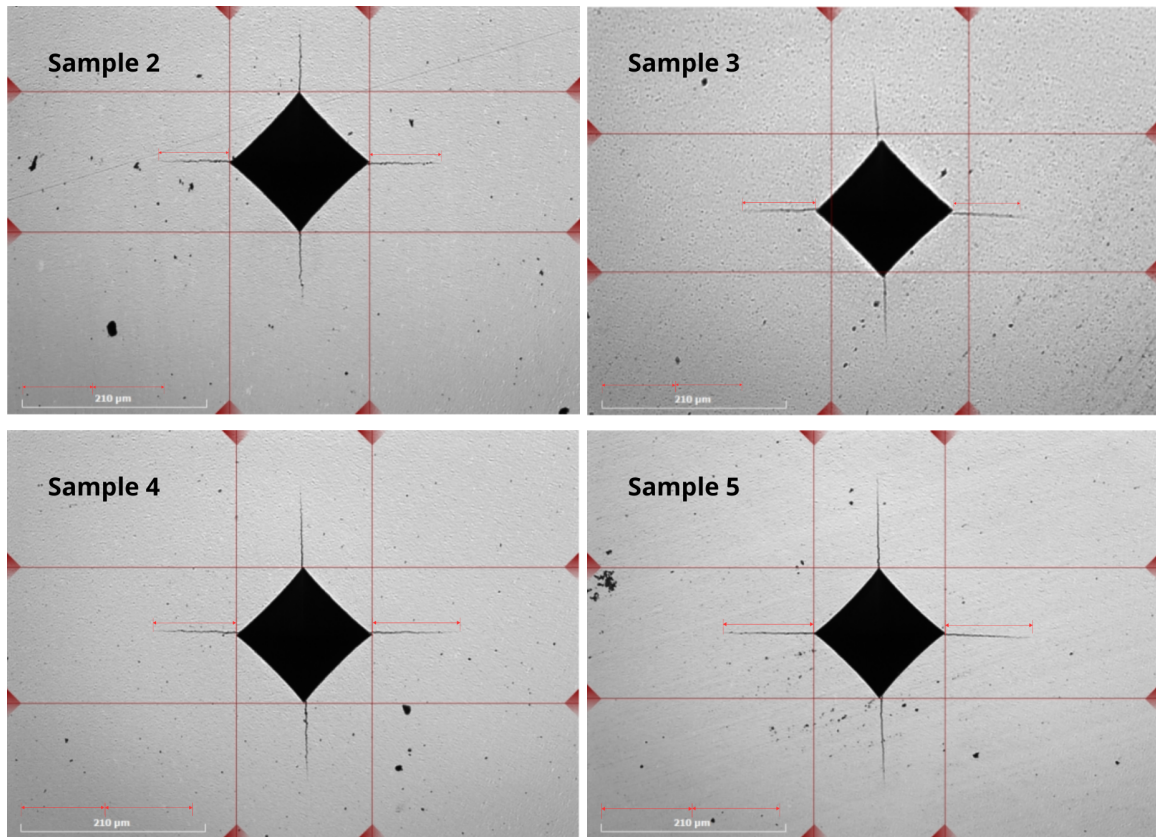
$$A_{\text{grain}} = N_{\text{pixels}} \cdot \text{stepsize}_x \cdot \text{stepsize}_y \quad d = 2 \cdot \sqrt{A/\pi}$$

F) Hardness comparison for WC-Co and WC-Fe-Ni-Co samples

**Table 4.** hardness and grain size data for WC-Co samples in figure 16 [30]

Hardness (HV)	Grain size ( $\mu\text{m}$ )	Hardness (HV)	Grain size ( $\mu\text{m}$ )
1717	1,13	1840	0,8
1533	0,99	2050	0,5
1500	1,09	1850	0,7
1478	1,04	1775	0,7
1416	1,51	1700	1,1
1370	1,95	1625	1,1
1710	1	1650	1,1
1860	0,7	1500	1,7
1680	1,2		

G) Crack length measurement for the samples



These crack length measures are used for figure 17 and 18

H) Crack length comparison for WC-Co and WC-Fe-Ni-Co samples

**Table 5.** crack length data for WC-Co samples on figure 19, calculated with literature data [15]

Hardness (HV30)	KIC (-)	P (kgf)	Crack (mm)
1857	9,7	30	0,4467
1756	9,1	30	0,4800
2100	7,9	30	0,7616
1925	8,6	30	0,5891
1850	9,2	30	0,4947
1765	9,2	30	0,4720
1796	9,1	30	0,4909
1680	8,5	30	0,5263
1635	8,2	30	0,5504
1698	8,5	30	0,5320
1756	9,7	30	0,4224
1661	9	30	0,4642
1661	8,9	30	0,4746
1643	8,9	30	0,4695
1591	9,6	30	0,3908
1660	9,8	30	0,3912
1643	9,6	30	0,4035
1608	8,8	30	0,4700
1608	9	30	0,4493
1565	9,5	30	0,3925
1608	9,4	30	0,4119
1540	10,1	30	0,3417
1557	9,5	30	0,3905
1608	9,3	30	0,4208
1589	10,5	30	0,3262
1574	9,7	30	0,3786
1557	8,8	30	0,4551

<i>1541</i>	<i>9,7</i>	<i>30</i>	<i>0,3707</i>
<i>1574</i>	<i>9,9</i>	<i>30</i>	<i>0,3635</i>
<i>1518</i>	<i>10,7</i>	<i>30</i>	<i>0,3001</i>
<i>1463</i>	<i>10,4</i>	<i>30</i>	<i>0,3062</i>
<i>1509</i>	<i>10,9</i>	<i>30</i>	<i>0,2875</i>
<i>1494</i>	<i>9,9</i>	<i>30</i>	<i>0,3450</i>
<i>1482</i>	<i>10,6</i>	<i>30</i>	<i>0,2985</i>
<i>1363</i>	<i>11,2</i>	<i>30</i>	<i>0,2459</i>
<i>1265</i>	<i>12,1</i>	<i>30</i>	<i>0,1956</i>
<i>1324</i>	<i>11,8</i>	<i>30</i>	<i>0,2152</i>
<i>1419</i>	<i>11,8</i>	<i>30</i>	<i>0,2307</i>
<i>1377</i>	<i>11,3</i>	<i>30</i>	<i>0,2441</i>
<i>1337</i>	<i>11,2</i>	<i>30</i>	<i>0,2413</i>
<i>1298</i>	<i>12</i>	<i>30</i>	<i>0,2040</i>
<i>1261</i>	<i>11,3</i>	<i>30</i>	<i>0,2235</i>
<i>1286</i>	<i>12,7</i>	<i>30</i>	<i>0,1805</i>
<i>1226</i>	<i>12,3</i>	<i>30</i>	<i>0,1834</i>
<i>1235</i>	<i>12,7</i>	<i>80</i>	<i>0,4622</i>
<i>1250</i>	<i>12,4</i>	<i>30</i>	<i>0,1840</i>
<i>1778</i>	<i>9,1</i>	<i>30</i>	<i>0,4860</i>
<i>1726</i>	<i>9,4</i>	<i>30</i>	<i>0,4421</i>
<i>1576</i>	<i>10,1</i>	<i>30</i>	<i>0,3497</i>
<i>1925</i>	<i>9,2</i>	<i>30</i>	<i>0,5148</i>
<i>1576</i>	<i>9,8</i>	<i>30</i>	<i>0,3714</i>
<i>1484</i>	<i>11,8</i>	<i>30</i>	<i>0,2412</i>
<i>1513</i>	<i>10,7</i>	<i>30</i>	<i>0,2991</i>